

## Article

# Enhancing the Terahertz Absorption Spectrum Based on the Low Refractive Index All-Dielectric Metasurface

Pingan Liu <sup>1</sup>, Wenping Li <sup>1</sup>, Naichang Chen <sup>2</sup>, Chan Ma <sup>3</sup>, Xiangjun Li <sup>3,\*</sup> and Dexian Yan <sup>3,\*</sup><sup>1</sup> Qingdao Qingyuanfengda Terahertz Technology Co., Ltd., Qingdao 266100, China<sup>2</sup> Institute of Wenzhou Yongliang Machinery Technology, Wenzhou 325000, China<sup>3</sup> Centre for THz Research, China Jiliang University, Hangzhou 310018, China

\* Correspondence: xiangjun\_li@cjlju.edu.cn (X.L.); yandexian1991@cjlju.edu.cn (D.Y.)

**Abstract:** We presented an angle-multiplexing low refractive index dielectric metasurface for terahertz absorption spectrum enhancement of lactose with high Q resonance properties. The unit cell structure of the acrylonitrile butadiene styrene (ABS) square structure is designed and optimized. The resonant peak shifts of the dielectric metasurface are analyzed by changing the incident angle of the terahertz wave. Then the  $\alpha$ -lactose films with different thicknesses are added to investigate the enhancement effect. The resonant peak amplitude of the angle-multiplexing low refractive index dielectric metasurface absorption spectrum changes greatly with the absorption spectrum of the samples. The results illustrate that the enhanced absorption spectrum formed by the linked envelope can be up to 45 times stronger than that without the unit cell structures and also exhibits a high-quality factor. The proposed dielectric metasurface provides great potential in enhancing the terahertz absorption spectrum.

**Keywords:** dielectric metasurface; angle-multiplexing; terahertz absorption spectrum enhancement



**Citation:** Liu, P.; Li, W.; Chen, N.; Ma, C.; Li, X.; Yan, D. Enhancing the Terahertz Absorption Spectrum Based on the Low Refractive Index All-Dielectric Metasurface. *Photonics* **2022**, *9*, 848. <https://doi.org/10.3390/photonics9110848>

Received: 16 October 2022

Accepted: 2 November 2022

Published: 10 November 2022

**Publisher's Note:** MDPI stays neutral with regard to jurisdictional claims in published maps and institutional affiliations.



**Copyright:** © 2022 by the authors. Licensee MDPI, Basel, Switzerland. This article is an open access article distributed under the terms and conditions of the Creative Commons Attribution (CC BY) license (<https://creativecommons.org/licenses/by/4.0/>).

## 1. Introduction

Terahertz wave usually refers to an electromagnetic wave with a frequency range of 0.1–10.0 THz (1 THz =  $10^{12}$  Hz), which has a better spatial resolution than the lower microwave wave and a stronger penetration than the upper infrared light [1]. Terahertz waves can directly detect the unique fingerprint of organic biomolecules and exhibit great application value in biosafety, security, environmental protection, and other fields [2]. However, the terahertz absorption spectrum measurements of trace matter are still very challenging. Current direct measurement of the terahertz absorption spectrum of solid samples based on the tablet-pressing technique usually requires several hundred milligrams to several grams of material. To measure the responses of the trace amount of samples to the terahertz waves, additional enhanced structures are needed to boost the interaction between the samples and the electromagnetic waves, such as photonic crystal fibers [3], resonant cavity [4], metal grating [5], metal split ring resonator [6], dielectric metasurface [7–11], and other structures. Similar to the structures used in the visible and infrared band [12–14], the metasurface structures composed of sub-wavelength structure arrays are the main class of sensitive structures [15,16].

Most of the current terahertz or other bands metasurface high sensitivity sensors are prepared based on the principle that the single-frequency resonance peak of the high Q resonant structure changes with the refractive index of the trace amount samples [17–20]. These high-Q structures can only enhance the interaction between the electromagnetic waves and the substance at a single frequency point and cannot identify the broad characteristic absorption spectrum of the trace analyte. The parametric multiplexed terahertz metasurface can utilize multiple metasurfaces with different-size unit structures or multiple incident wave angles to generate a series of resonance peaks to enhance the interaction between electromagnetic waves and matter. In particular, the amplitudes of these resonance

peaks change with the absorption spectrum of the samples, the envelope is consistent with the shape of the characteristic absorption spectrum of the samples, and the amplitude is greatly increased compared with the unenhanced absorption spectrum. This multiplexing mechanism can directly and significantly enhance the terahertz fingerprint absorption spectrum of trace amounts of samples, demonstrating great application value.

In 2019, Leitis et al. combined the high-Q dielectric metasurface supporting the bound state in the continuum (BIC) with angle multiplexing; the produced resonant peaks can cover a wider band in the mid-infrared range [21]. In particular, the peak amplitude changes drastically with the absorption spectrum of the trace amount of samples. The amplitude of the analyte absorption spectrum composed of the resonance peak envelope is 50 times that of the direct measurement, and the detection sensitivity is about 3000 molecules/ $\mu\text{m}^2$ . In their other work, the absorption spectrum was enhanced 60-fold based on geometric multiplexing [22]. Zhong et al. obtained the terahertz absorption spectrum of a 5  $\mu\text{m}$  thick lactose film based on a similar structure using angle multiplexing; the detection sensitivity reached 59.35 mg/ $\text{cm}^2$  [23]. However, the structure requires thinning of quartz wafer and bonding with quartz substrate, and the fabricating process is complex. Zhu et al. enhanced the absorption spectrum of hBN in the infrared band, with an increase of about 31.6 times [24]. The absorption spectrum of lactose and 2,4-DNT was enhanced about 20 times in the terahertz regime [25]. Unfortunately, the building process also needs high-cost photo-lithography technology.

In this paper, a metasurface structure with quartz substrate and acrylonitrile butadiene styrene (ABS) microstructures is proposed, which has a low-refractive index and high Q resonance characteristics. The resonance peak frequencies of the metasurface response spectrum related to different terahertz wave incident angles can cover 0.5–0.57 THz. Based on the multipole decomposition method, it is confirmed that the resonances at the incident angles of 15°, 25°, 35°, and 45° are dominated by the magnetic toroidal dipole. When the metasurface structure is covered with the 1–3  $\mu\text{m}$  lactose film as the analyte, the amplitude of the resonance peak corresponding to different incident angles changes obviously with the absorption spectrum of the analyte, and the absorption spectrum composed of the envelope of the resonant peaks is about 45 times higher than the directly calculated value without the metasurface structure. The designed metasurface exhibits great potential for enhancing the terahertz absorption spectrum, which can be used to detect trace organic substances with different characteristics. Furthermore, the fabrication process is relatively simple with 3D printing technology and easy to be applied in practice.

## 2. Structure and Concept

The dielectric metasurface structure designed in this paper is shown in Figure 1a, which is composed of two square structures periodically arranged on the substrate. The material of the microstructures is ABS, which has the advantages of low refractive index, low cost, and high Q resonance characteristics. The structure of two squares in the unit cell can effectively improve the quality factor of the metasurface because they can support the bound states in a continuum with a higher Q value [26]. The use of this material can reduce the manufacturing difficulty of 3D printing and is conducive to practical applications. This metasurface can be fabricated by the commercial 3D printer using the heating extrusion method with ABS. The refractive index of ABS is about 1.67 [27] in the terahertz band. The substrate material is  $\text{SiO}_2$ , with a refractive index of 1.95 [28,29]. Figure 1b depicts the unit cell structure of the dielectric metasurface, and the geometric parameters are  $P_x = 400 \mu\text{m}$ ,  $P_y = 400 \mu\text{m}$ ,  $w = 180 \mu\text{m}$ ,  $g = 20 \mu\text{m}$ ,  $h = 500 \mu\text{m}$ , and  $t = 85 \mu\text{m}$ . To investigate the terahertz absorption spectrum enhancement ability of the metasurface, the FEM method is treated to study the response characteristics in the terahertz band. In the simulation process, the  $x$  and  $y$  directions are set as the periodic boundaries, and the  $z$  direction is set as the open boundary. The terahertz wave with TM polarized state is incident on the metasurface with the incidence angle of  $\alpha$ .

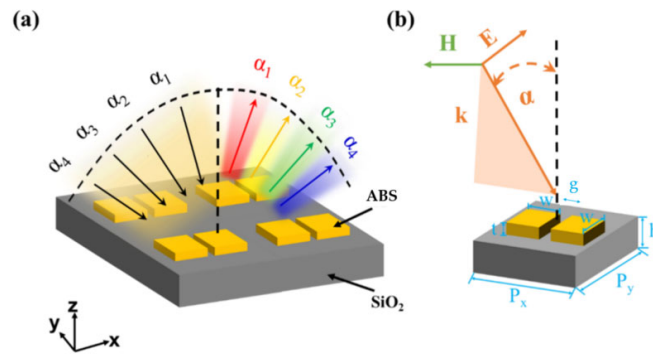


**Figure 1.** Schematic of terahertz absorption enhancement detection based on the angle-multiplexing of the dielectric metasurface. (a) Angle-multiplexing principle of dielectric metasurface with the several incidence angles of  $\alpha$ , such as  $\alpha_1$ – $\alpha_4$ ; (b) The unit cell structure of the metasurface. The transverse magnetic field H of TM polarized incident wave is along the y-axis.

### 3. Results Unit Cell Structure Design and Optimization

First, we investigated the effects of the terahertz wave incident angle and the geometric parameters of unit cell structure on the form of a high Q resonance peak in the reflection spectrum. The high Q resonant peak means that the electromagnetic wave with the resonant peak frequency generates a strong local field around the micro-structure of the dielectric metasurface, which can enhance the interaction between the electromagnetic wave and the trace amount of samples. This phenomenon is the main physical basis for the subsequent absorption spectrum enhancement. Figure 2a,b illustrate the reflection spectrum of the metasurface in the frequency band of 0.5–0.57 THz with different terahertz wave incident angles and the  $w$  of the metasurface unit cell structure. The incident angle  $\alpha$  of the terahertz wave is changed in the range of 20° to 40°, and the width  $w$  of the square varies from 120  $\mu\text{m}$  to 200  $\mu\text{m}$ . By optimizing the unit cell structure, the resonant peak is located around 0.53 THz with a high Q value so that the resonant peak can cover a wider frequency band centered at 0.53 THz by angle scanning. When  $\alpha$  scans from 20° to 40°, the resonant peak exhibits a blue shift trend, essentially covering the range of 0.5–0.57 THz. When  $w$  changes from 120  $\mu\text{m}$  to 200  $\mu\text{m}$ , the resonant peak demonstrates the red-shift trend, and the range of the shift is relatively small. The reason for the blue shift of the resonant frequency is that the equivalent resonant volume increases due to the increase of the incident angles during the scanning process, resulting in an increase of the resonant frequency [21].

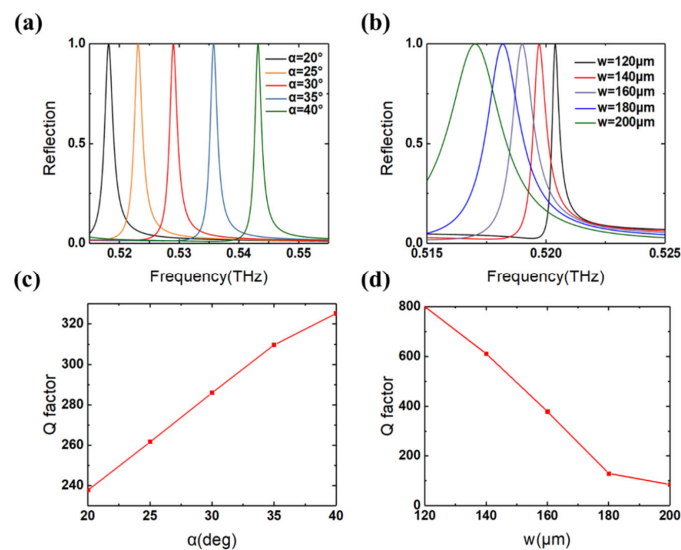


**Figure 2.** Effects of terahertz wave incident angles and unit cell structure parameters on the reflection spectrum and Q value change. (a,c)  $\alpha = 20$ – $40^\circ$ ; (b,d)  $w = 120$ – $200 \mu\text{m}$ .

In addition, the effects of terahertz wave incidence angles and unit cell structure parameters on the Q value of the metasurface reflection spectrum are investigated and shown in Figure 2c,d. When the incident angle  $\alpha$  increases from  $20^\circ$  to  $40^\circ$ , the Q value gradually increases and remains above 200, indicating that the unit cell structure provides a better electromagnetic field confinement ability. Then when  $w$  increases from  $120\ \mu\text{m}$  to  $200\ \mu\text{m}$ , the Q value greatly decreases, and the electromagnetic field confinement ability weakens. The Q value can be further improved by optimizing the geometry parameters, which will achieve better-enhancing performance for the trace sample absorption spectrum in the future, though the Q value is relatively smaller than those structures with higher refractive index material such as Si and GaAs.

#### 4. Discussion

Here, the  $\alpha$ -lactose with a characteristic absorption peak around 0.53 THz is used as the analyte to simulate and verify the terahertz absorption spectrum enhancement metasurface structure. And it is relatively inert, nonpoisonous, and easily available. Figure 3a gives the real and imaginary parts of the  $\alpha$ -lactose dielectric constant calculated based on the Lorentzian model as follows [30]:

$$\epsilon_r = \epsilon_\infty + \frac{\Delta\epsilon_p\omega_p^2}{\omega_p^2 - \omega^2 - j\gamma_p\omega} \tag{1}$$

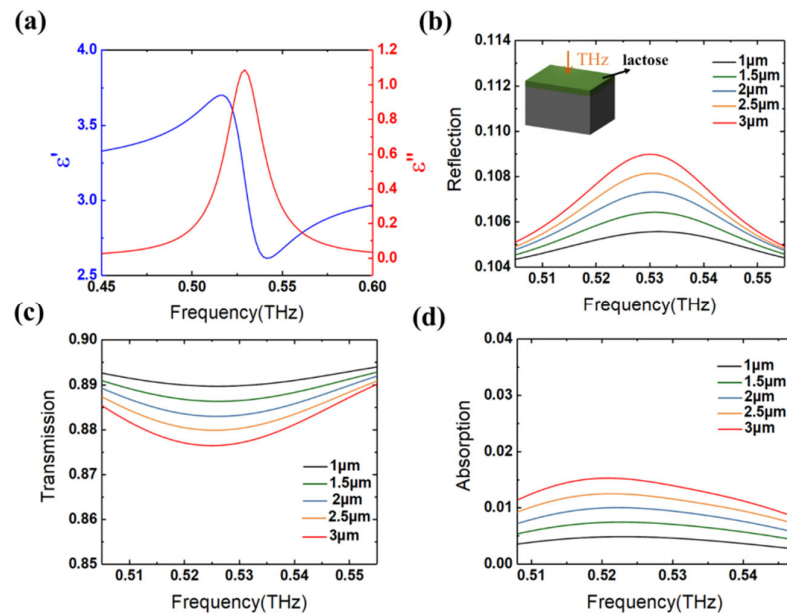


**Figure 3.** The dielectric constant of the  $\alpha$ -lactose and the response characteristics of the lactose films coated on the metasurface. (a) Dielectric constant of  $\alpha$ -lactose; (b) reflection, (c) transmission, and (d) absorption of the lactose-coated quartz substrate.

Here,  $\epsilon_\infty = 2.08$  denotes the off-resonance background permittivity of lactose,  $\omega_p/2\pi = 0.53\ \text{THz}$ , and  $\gamma_p/2\pi = 25.2\ \text{GHz}$  is the angular frequency and damping rate of the first absorption oscillation, respectively, and  $\Delta\epsilon_p = 6.54 \times 10^{-3}$  is the oscillation strength factor. The corresponding real and imaginary parts of permittivity during 0.45–0.6 THz are illustrated in Figure 3a.

We first coat the  $\alpha$ -lactose films with a thickness of 1–3  $\mu\text{m}$  directly on the quartz substrate. In addition, then the reflection, transmission, and absorption are calculated and shown in Figure 3b–d. It can be seen from Figure 3d that the directly measured terahertz absorption of the thin film sample is very small, and it is only about 0.015 for the  $\alpha$ -lactose film with a thickness of 3  $\mu\text{m}$ . This is easily overwhelmed by the noise in actual measurement and can not be measured. Therefore, metasurfaces are required to provide

locally enhanced electromagnetic fields to boost the interaction between the electromagnetic waves and the samples.

As shown in Figure 4a, the  $\alpha$ -lactose films with a thickness of 3  $\mu\text{m}$  are coated on the surface of the unit cell structure, and the terahertz wave with TM polarization is incident on the metasurface with the incident angle increasing from  $20^\circ$  to  $45^\circ$  with a step of  $1^\circ$ . As illustrated in Figure 4b,c, the resonant peak amplitudes of the reflection coefficient and transmission coefficient of the metasurface remain unchanged with the incident angle when the lactose films are not coated. From Figure 4d,e, when the  $\alpha$ -lactose films with a thickness of 3  $\mu\text{m}$  are coated on the metasurface, the resonant peak amplitudes of the reflection and transmission change significantly with the incident angle. Figure 4f shows the absorption rates of the lactose-coated metasurface with different incident angles, and the envelope built by linking these resonant peaks can serve as the enhanced lactose absorption spectrum. Compared with the absorption spectrum measured directly without the dielectric metasurface structures, the peak amplitude of the absorption spectrum with the metasurface structure is enhanced by a factor of 24.8. The above results demonstrate that the terahertz absorption spectrum enhancement effect of the metasurface structure here is obvious.

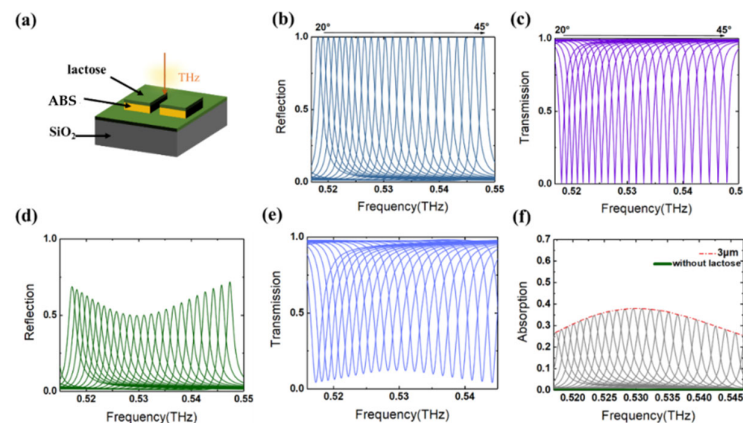


**Figure 4.** Terahertz absorption spectrum enhancement of the dielectric metasurface without and with  $\alpha$ -lactose coatings based on the angle-multiplexing. (a) The unit cell structure of the dielectric metasurface coated with  $\alpha$ -lactose films; (b) reflection and (c) transmission of the metasurface without  $\alpha$ -lactose coatings; (d) reflection and (e) transmission of the metasurface coated with 3  $\mu\text{m}$   $\alpha$ -lactose; (f) absorption of the metasurface coated with 3  $\mu\text{m}$   $\alpha$ -lactose compared with the no-coating situation.

To further illustrate the absorption spectrum enhancement mechanism of the dielectric metasurface proposed in this paper, the electric field intensity distributions of the resonant frequencies for the unit cell structure with a 3  $\mu\text{m}$  lactose film at four different incident angles are investigated and shown in Figure 5. The four studied angles are  $15^\circ$ ,  $25^\circ$ ,  $35^\circ$ , and  $45^\circ$ , corresponding to the resonant frequencies of 0.511 THz, 0.527 THz, 0.534 THz, and 0.545 THz. The same field intensity color bars are used in the four plots. When the resonant frequency is close to the lactose characteristic absorption frequency of 0.529 THz, the field strength distributions around the square structures at 0.527 THz (Figure 5b) and 0.534 THz (Figure 5c) are higher than the field distributions of the frequencies of 0.511 THz (Figure 5a) and 0.545 THz (Figure 5d). The above results indicate that the absorption peak of the lactose and the resonance peak of the dielectric metasurface is effectively coupled, and the change of the lactose absorption can significantly affect the electric field strength of the resonance frequency, enhancing the terahertz absorption spectrum of lactose.

To study the electromagnetic and scattering properties of the designed metasurface, scattered Cartesian powers for multipole moments are calculated based on the induced current inside of the nanoparticle [31–33]. Thus, the multipole contributions can be identified. The detailed expressions can be obtained in our previous work [34]. When the TM-polarized terahertz wave incidents on the metasurface, qualitative analyses of the

resonant situation with four different incident angles ( $15^\circ$ ,  $25^\circ$ ,  $35^\circ$ ,  $45^\circ$ ) are performed, and the results are illustrated in Figure 6. The P, M, QE, QM, ET, and MT are the electric dipole, magnetic dipole, electric quadrupole, magnetic quadrupole, electric toroidal dipole, and magnetic toroidal dipole, respectively. In Figure 6, the results demonstrate the resonance is dominated by the magnetic toroidal dipole. It can be concluded that the mode is a magnetic toroidal dipole mode between single squares.

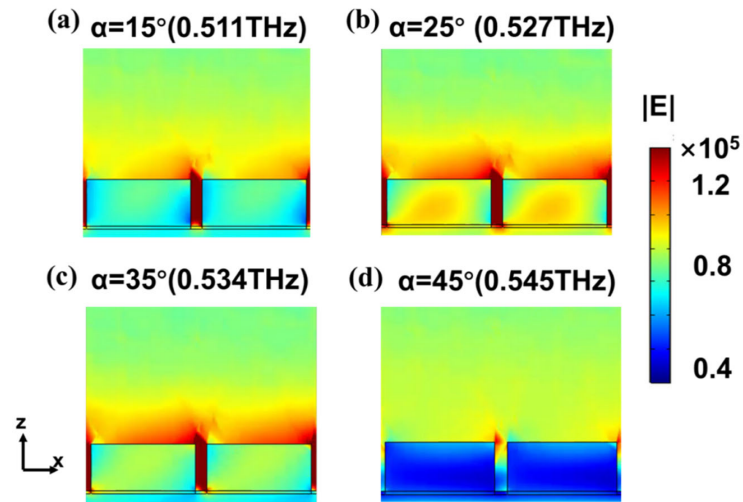


**Figure 5.** Electric field distributions of the lactose film-coated dielectric metasurface with different incident angles. (a) Incident angle of  $15^\circ$  with a resonant frequency of 0.511 THz; (b) Incident angle of  $25^\circ$  with a resonant frequency of 0.527 THz; (c) Incident angle of  $35^\circ$  with a resonant frequency of 0.534 THz; (d) Incident angle of  $45^\circ$  with the resonant frequency of 0.545 THz.

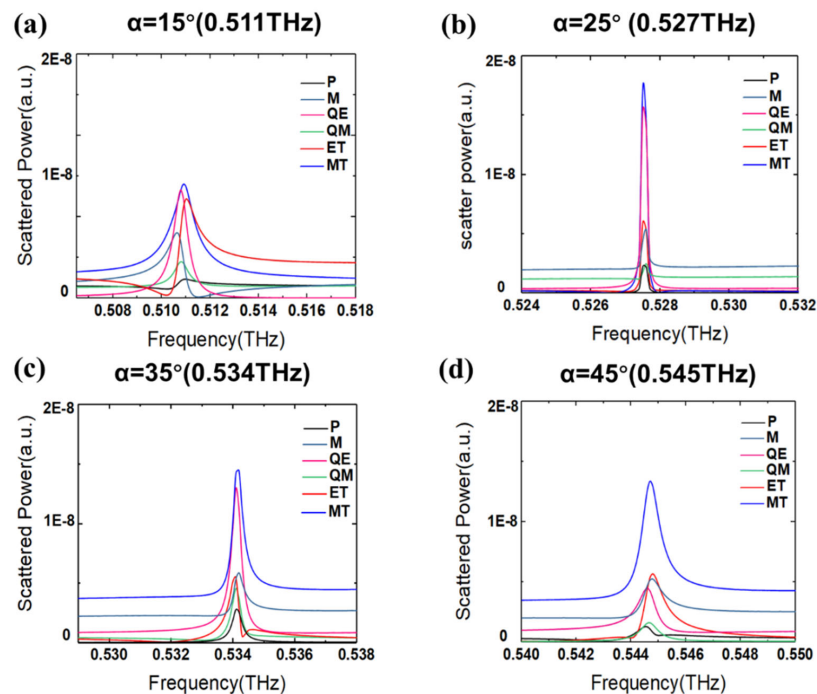


**Figure 6.** Calculated scattering powers of multipoles decomposition for the studied metasurface, where P, M, QE, QM, ET, and MT are the electric dipole, magnetic dipole, electric quadrupole, magnetic quadrupole, electric toroidal dipole, and magnetic toroidal dipole, respectively. (a) Incident angle of  $15^\circ$  with a resonant frequency of 0.511 THz; (b) Incident angle of  $25^\circ$  with a resonant frequency of 0.527 THz; (c) Incident angle of  $35^\circ$  with a resonant frequency of 0.534 THz; (d) Incident angle of  $45^\circ$  with the resonant frequency of 0.545 THz.

Next, we investigate the influence of lactose thickness on the terahertz absorption spectrum enhancement. Here, the absorption spectrum enhancement effects of the metasurface with 1–3  $\mu\text{m}$  lactose film coatings have been investigated. The enhanced absorption spectrum of each lactose thickness can be achieved based on the extraction of dielectric metasurface resonance peaks and envelop linking, as shown in Figure 7a–e, with the thickness of lactose increasing from 1  $\mu\text{m}$  to 3  $\mu\text{m}$  in a step of 0.5  $\mu\text{m}$ . Figure 7f shows the comparison results of the enhanced absorption spectrum with different lactose thicknesses. The amplitude of the enhanced absorption spectrum increases with the lactose thickness, and the increasing degree gradually becomes smaller, basically consistent with the Lambert-Beer law. Compared with the lactose film of the same thickness without enhanced structure, the absorption spectra are enhanced by 45 times, 37.1 times, 32.13 times, 31.78 times, and 24.8 times for the lactose thicknesses of 1  $\mu\text{m}$  to 3  $\mu\text{m}$ , respectively.

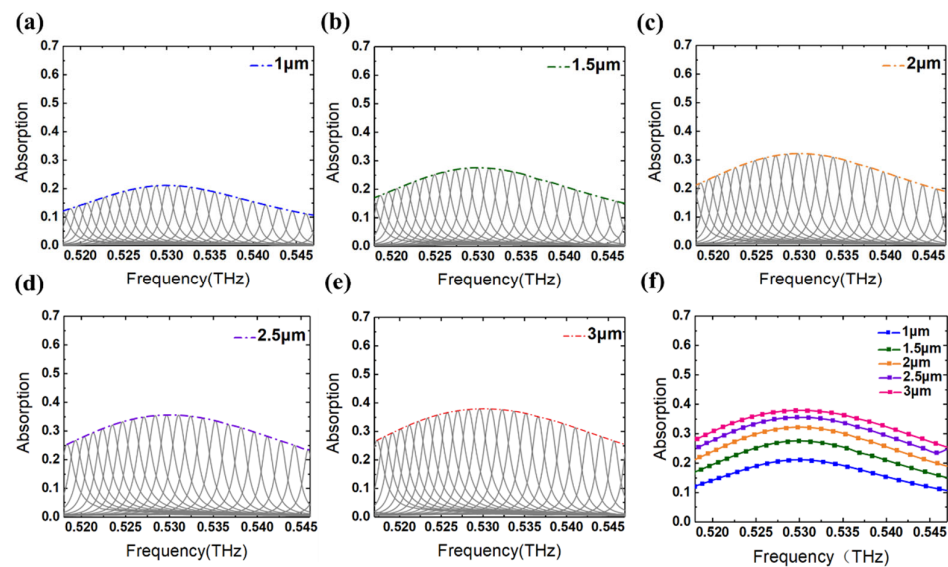


**Figure 7.** The enhanced absorption spectrum of the dielectric metasurface coated with different thicknesses of lactose. (a) 1  $\mu\text{m}$ ; (b) 1.5  $\mu\text{m}$ ; (c) 2  $\mu\text{m}$ ; (d) 2.5  $\mu\text{m}$ ; (e) 3  $\mu\text{m}$ ; (f) Comparison results.

At last, we compared our work with the reported results of dielectric metasurfaces or gratings with different multiplexing technologies in Table 1. It is demonstrated that the proposed metasurface has better enhancement performance than its terahertz counterpart.

**Table 1.** Comparison of absorption spectra enhancement performances of present metasurfaces or gratings based on multiplexing technology and our designed structure.

Ref.	Cell Structure	Analyte	Multiplexing Mode	Working Band	Absorbance Peak Enhancement Factor
[21]	Dielectric Pair Pillars	PMMA	Angle of incident	Mid-infrared	~50 times
[22]	Dielectric Pair Pillars	PMMA	Geometry	Mid-infrared	~60 times
[24]	Dielectric Grating	hBN	Angle of incident	Mid-infrared	~30 times
[25]	Dielectric Grating	$\alpha$ -lactose	Angle of incident	THz	~20 times
This work	Dielectric Metasurface	lactose	Angle of incident	THz	~45 times

### 5. Conclusions

In conclusion, a novel scheme for enhancing the terahertz absorption spectrum of trace amount samples based on low refractive index dielectric metasurface is designed.

This method is realized by treating the angle multiplexing operation. The metasurface substrate is quartz, and the cuboid unit cell structure is ABS polyamide. The resonant peak frequencies of the metasurface structures corresponding to different terahertz wave incident angles can cover the frequency range of 0.50–0.57 THz, and the Q factor is higher than 100. When the lactose films with thicknesses of 1–3  $\mu\text{m}$  are coated on the metasurface, the amplitude of the resonance peak corresponding to different incident angles varies substantially with the absorption spectrum of the samples. The absorption spectrum composed of the envelope is up to 45 times stronger than the directly calculated value. The results demonstrate that the designed dielectric metasurface shows great potential to enhance the terahertz absorption spectrum through angle multiplexing, which can be optimized to detect a trace amount of samples with different characteristic peaks.

**Author Contributions:** Data Curation, X.L.; Conceptualization, D.Y.; software, X.L. and C.M.; investigation, C.M. and P.L.; resources, W.L. and N.C.; writing—original draft preparation, D.Y.; writing—review and editing, X.L. Funding acquisition, X.L. All authors have read and agreed to the published version of the manuscript.

**Funding:** This research was funded by National Key R&D Program of China (2021YFF0600300) and Natural Science Foundation of Zhejiang Province (LQ20F010009).

**Institutional Review Board Statement:** Not applicable.

**Informed Consent Statement:** Not applicable.

**Data Availability Statement:** Not applicable.

**Conflicts of Interest:** The authors declare no conflict of interest.

## References

1. Tonouchi, M. Cutting-edge terahertz technology. *Nat. Photon.* **2007**, *1*, 97–105. [[CrossRef](#)]
2. Yan, D.; Wang, Y.; Qiu, Y.; Feng, Q.; Li, X.; Li, J.; Qiu, G.; Li, J. A Review: The Functional Materials-Assisted Terahertz Metamaterial Absorbers and Polarization Converters. *Photonics* **2022**, *9*, 335. [[CrossRef](#)]
3. Sultana, J.; Islam, M.S.; Ahmed, K.; Dinovitser, A.; Ng, B.W.H.; Abbott, D. Terahertz detection of alcohol using a photonic crystal fiber sensor. *Appl. Opt.* **2018**, *57*, 2426–2433. [[CrossRef](#)] [[PubMed](#)]
4. Yee, C.M.; Sherwin, M.S. High-Q terahertz microcavities in quartz photonic crystal slabs. *Appl. Phys. Lett.* **2009**, *94*, 4648. [[CrossRef](#)]
5. Wang, Y.; Li, X.; Lang, T.; Jing, X.; Hong, Z. Multiband guided-mode resonance filter in bilayer asymmetric metallic gratings. *Opt. Laser Technol.* **2018**, *103*, 135–141. [[CrossRef](#)]
6. Gupta, M.; Srivastava, Y.K.; Manjappa, M.; Singh, R. Sensing with Toroidal Metamaterial. *Appl. Phys. Lett.* **2017**, *110*, 121108. [[CrossRef](#)]
7. Yan, D.; Li, X.; Ma, C.; Qiu, G.; Cao, M.; Li, J.; Guo, S. Terahertz Refractive Index Sensing Based on Gradient Metasurface Coupled Confined Spoof Surface Plasmon Polaritons Mode. *IEEE Sens. J.* **2021**, *22*, 324–329. [[CrossRef](#)]
8. Chen, H.; Chen, Z.; Yang, H.; Wen, L.; Yi, Z.; Zhou, Z.; Dai, B.; Zhang, J.; Wu, X.; Wu, P. Multi-mode surface plasmon resonance absorber based on dart-type single-layer graphene. *RSC Adv.* **2022**, *12*, 7821–7829. [[CrossRef](#)]
9. Zheng, Z.; Zheng, Y.; Luo, Y.; Yi, Z.; Zhang, J.; Liu, Z.; Yang, W.; Yu, Y.; Wu, X.; Wu, P. A switchable terahertz device combining ultra-wideband absorption and ultra-wideband complete reflection. *Phys. Chem. Chem. Phys.* **2022**, *24*, 2527–2533. [[CrossRef](#)]
10. Zhao, J.; Cheng, Y. Temperature-Tunable Terahertz Perfect Absorber Based on All-Dielectric Strontium Titanate (STO) Resonator Structure. *Adv. Theory Simul.* **2022**, 2200520. [[CrossRef](#)]
11. Li, Z.; Cheng, Y.; Luo, H.; Chen, F.; Li, X. Dual-band tunable terahertz perfect absorber based on all-dielectric InSb resonator structure for sensing application. *J. Alloys Compd.* **2022**, 925, 166617. [[CrossRef](#)]
12. Long, Z.; Liang, Y.; Feng, L.; Zhang, H.; Liu, M.; Xu, T. Low-cost and high sensitivity glucose sandwich detection using a plasmonic nanodisk metasurface. *Nanoscale* **2020**, *12*, 10809–10815. [[CrossRef](#)]
13. Yesilkoy, F.; Arvelo, E.R.; Jahani, Y.; Liu, M.; Tittl, A.; Cevher, V.; Kivshar, Y.; Altug, H. Ultrasensitive Hyperspectral Imaging and Biodetection Enabled by Dielectric Metasurfaces. *Nat. Photon.* **2019**, *13*, 390–396. [[CrossRef](#)]
14. Liang, Y.; Cui, W.; Li, L.; Yu, Z.; Peng, W.; Xu, T. Large-scale plasmonic nanodisk structures for a high sensitivity biosensing platform fabricated by transfer nanoprinting. *Adv. Opt. Mater.* **2019**, *7*, 1801269. [[CrossRef](#)]
15. Feng, Q.Y.; Yan, D.X.; Li, X.J.; Li, J.N. Realization of absorption, filtering, and sensing in a single metamaterial structure combined with functional materials. *Appl. Opt.* **2022**, *61*, 4336–4343. [[CrossRef](#)]
16. Samadi, M.; Abshari, F.; Algorri, J.F.; Varona, P.; Cobo, L.; Higuera, J.; Pena, J.; Zografopoulos, D.; Dell’Olio, F. All-Dielectric Metasurface Based on Complementary Split-Ring Resonators for Refractive Index Sensing. *Photonics* **2022**, *9*, 130. [[CrossRef](#)]

17. Chen, J.; Kuang, Y.; Gu, P.; Feng, S.; Zhu, Y.; Tang, C.; Guo, Y.; Liu, Z.; Gao, F. Strong magnetic plasmon resonance in a simple metasurface for high-quality sensing. *J. Lightwave Technol.* **2021**, *39*, 4525–4528. [[CrossRef](#)]
18. Tumashov, M.A.; del Risco, J.P.; Glybovski, S.B.; Sayanskiy, A.D.; Kuznetsov, S.A.; Baena, J.D. Comparison of angular-selective metasurfaces as tools for sub-THz single-frequency sensing. *J. Phys. Conf. Ser.* **2021**, *2015*, 012158. [[CrossRef](#)]
19. Wang, Y.L.; Han, Z.H.; Du, Y.; Qin, J.Y. Ultrasensitive terahertz sensing with high-Q toroidal dipole resonance governed by bound states in the continuum in all-dielectric metasurface. *Nanophotonics* **2021**, *10*, 1295–1307. [[CrossRef](#)]
20. Tognazzi, A.; Rocco, D.; Gandolfi, M.; Locatelli, A.; Carletti, L.; De Angelis, C. High Quality Factor Quartz Membrane Metasurface for Intensity-Based Refractive Index Sensing. *Optics* **2021**, *2*, 193–199. [[CrossRef](#)]
21. Leitis, A.; Tittl, A.; Liu, M.; Lee, B.H.; Gu, M.B.; Kivshar, Y.S.; Altug, H. Angle-multiplexed all-dielectric metasurfaces for broadband molecular fingerprint retrieval. *Sci. Adv.* **2019**, *5*, 9. [[CrossRef](#)] [[PubMed](#)]
22. Tittl, A.; Leitis, A.; Liu, M.; Yesilkoy, F.; Choi, D.-Y.; Neshev, D.N.; Kivshar, Y.S.; Altug, H. Imaging-Based Molecular Barcoding with Pixelated Dielectric Metasurfaces. *Science* **2018**, *360*, 1105–1109. [[CrossRef](#)] [[PubMed](#)]
23. Zhong, Y.; Du, L.; Liu, Q.; Zhu, L.; Meng, K.; Zou, Y.; Zhang, B. Ultrasensitive specific sensor based on all-dielectric metasurfaces in the terahertz range. *RSC Adv.* **2020**, *10*, 33018–33025. [[CrossRef](#)] [[PubMed](#)]
24. Xie, Y.; Liu, X.; Li, F.; Zhu, J.; Feng, N. Ultra-wideband enhancement on mid-infrared fingerprint sensing for 2D materials and analytes of monolayers by a metagratings. *Nanophotonics* **2020**, *9*, 2927–2935. [[CrossRef](#)]
25. Zhu, J.; Jiang, S.; Xie, Y.; Li, F.; Du, L.; Meng, K.; Zhu, L.; Zhou, J. Enhancing terahertz molecular fingerprint detection by a dielectric metagrating. *Opt. Lett.* **2020**, *45*, 2335–2338. [[CrossRef](#)]
26. Chen, X.; Fan, W. Tunable bound states in the continuum in all-dielectric terahertz metasurfaces. *Nanomaterials* **2020**, *10*, 623. [[CrossRef](#)]
27. Zhai, M.; Locquet, A.; Citrin, D.S. Terahertz Dielectric Characterization of Low-Loss Thermoplastics for 6G Applications. *Int. J. Wirel. Inform. Netw.* **2022**, *29*, 269–274. [[CrossRef](#)]
28. You, B.; Peng, C.-C.; Jhang, J.-S.; Chen, H.-H.; Yu, C.-P.; Lai, W.-C.; Liu, T.-A.; Peng, J.-L.; Lu, J.-L. Terahertz plasmonic waveguide based on metal rod arrays for nanofilm sensing. *Opt. Express* **2014**, *22*, 11340–11350. [[CrossRef](#)]
29. Ma, Y.; Li, J.; Han, Z.; Maeda, H.; Ma, Y. Bragg-mirror-assisted high-contrast plasmonic interferometers: Concept and potential in terahertz sensing. *Nanomaterials* **2020**, *10*, 1385. [[CrossRef](#)]
30. Li, X.; Ma, C.; Yan, D.; Guo, S.; Zhang, L.; Yang, J.; Zhao, Y.; Zhou, W. Enhanced trace-amount terahertz vibrational absorption spectroscopy using surface spoof polarization in metasurface structures. *Opt. Lett.* **2022**, *47*, 2446–2449. [[CrossRef](#)]
31. Basharin, A.A.; Kafesaki, M.; Economou, E.N.; Soukoulis, C.M.; Fedotov, V.A.; Savinov, V.; Zheludev, N.I. Dielectric Metamaterials with Toroidal Dipolar Response. *Phys. Rev. X* **2015**, *5*, 011036. [[CrossRef](#)]
32. Radescu, E.E.; Vaman, G. Exact calculation of the angular momentum loss, recoil force, and radiation intensity for an arbitrary source in terms of electric, magnetic, and toroid multipoles. *Phys. Rev. E* **2002**, *65*, 046609. [[CrossRef](#)]
33. Savinov, V.; Fedotov, V.A.; Zheludev, N.I. Toroidal dipolar excitation and macroscopic electromagnetic properties of metamaterials. *Phys. Rev. B* **2014**, *89*, 205112. [[CrossRef](#)]
34. Li, X.; Yin, J.; Liu, Z.; Wang, Y.; Hong, Z. Tailoring the excitation of two kinds of toroidal dipoles in all-dielectric metasurfaces. *Optik* **2020**, *201*, 163502. [[CrossRef](#)]